0254-6124/2012/32(2)-170–12 *Chin. J. Space Sci.* 空间科学学报

Zhang Yanyan, Feng Xueshang, Jiang Chaowei, Zhou Yufen. Application of ADER scheme in MHD simulation. *Chin. J. Space Sci.*, 2012, **32**(2): 170-181

Application of ADER Scheme in MHD Simulation*

ZHANG Yanyan[1,2] FENG Xueshang[1] JIANG Chaowei[1,2] ZHOU Yufen[1]

1(*State Key Laboratory of Space Weather, Center for Space Science and Applied Research, Chinese Academy of Sciences, Beijing* 100190)

2(*Graduate University of Chinese Academy of Sciences, Beijing* 100049)

Abstract The Arbitrary accuracy Derivatives Riemann problem method (ADER) scheme is a new high order numerical scheme based on the concept of finite volume integration, and it is very easy to be extended up to any order of space and time accuracy by using a Taylor time expansion at the cell interface position. So far the approach has been applied successfully to flow mechanics problems. Our objective here is to carry out the extension of multidimensional ADER schemes to multidimensional MHD systems of conservation laws by calculating several MHD problems in one and two dimensions: (i) Brio-Wu shock tube problem, (ii) Dai-Woodward shock tube problem, (iii) Orszag-Tang MHD vortex problem. The numerical results prove that the ADER scheme possesses the ability to solve MHD problem, remains high order accuracy both in space and time, keeps precise in capturing the shock. Meanwhile, the compared tests show that the ADER scheme can restrain the oscillation and obtain the high order non-oscillatory result.

Key words ADER scheme, Generalized Riemann problem, MHD numerical simulation, HLL scheme

Classified Index P 353

0 Introduction

The classical Riemann problem is the Cauchy problem for a system of hyperbolic conservation laws, with initial condition consisting of two constant states separated by a discontinuity. The self-similar solution of this Riemann problem was first used by Godunov[1−2] to construct his first-order upwind numerical flux. Since then, methods to solve the classical Riemann problem have been studied, for example, in Ref.[3]. One of the developed methods is to extend the local Riemann problem to the Generalized Riemann problem at cell interface position. The so-call Generalized Riemann problem, in which the initial condition consists of two polynomials of the first degree (vectors) separated by a discontinuity at the interface, was first constructed by Ben-Artzi *et al.*[4] in one dimension. According to Toro's concept of the Generalized Riemann problem[5], the initial condition consists of two kth order polynomial functions, which are denoted as the corresponding Generalized Riemann problem by GRP_k. For example, GRP_0 means that all first and

* Supported by the National Natural Science Foundation of China (40904050, 40874077), and the Specialized Research Fund for State Key Laboratories

Received January 20, 2011. Revised August 10, 2011

E-mail: yyzhang@spaceweather.ac.cn

higher-order spatial derivatives of the initial condition for the GRP away from the origin vanish identically, which corresponds to the classical piece-wise constant data Riemann problem. Similarly, GRP_1 means that all second and higher-order spatial derivatives of the initial condition for the GRP away from the origin vanish identically, which corresponds to the piece-linear data Riemann problem. The most general case is that the initial conditions are two arbitrary but infinitely differentiable functions, which are denoted by GRP_∞.

A major simplification to the GRP methodology comes with the Modified GRP (MGRP) scheme, proposed by Toro *et al.*[6] In this scheme the GRP is solved by two conventional Riemann problems, namely one non-linear problem for the leading term for state variables and one linear problem for gradients of state variables. The Arbitrary accuracy Derivatives Riemann problem method (ADER) approach can be regarded as a further development of the MGRP scheme in that it breaks the barrier of second-order accuracy and allows the construction of arbitrarily high-order accurate schemes, both in time and space. This approach was put forward firstly by Toro and his collaborators[7], where they achieved 10th order of accuracy in both space and time. The ADER scheme has been applied successfully to the hydrodynamic systems. Titarev *et al.*[3,5,8,15] applied this scheme to the scalar advection-reaction-diffusion equations. Toro *et al.*[9] used TVD fluxes for the high-order ADER schemes. Toro *et al.*[10−14] used this scheme for linear and non-linear hyperbolic conservation laws from one- to three-dimensional hydrodynamic problem. Motivated by the ADER's successful application to hydrodynamic problem, we try to implement the scheme for MHD simulation. We apply the scheme to several MHD problems which are calculated in one and two dimensions: (i) Brio-Wu shock tube problem, (ii) Dai-Woodward shock tube problem, (iii) Orszag-Tang MHD vortex problem. The numerical results show that the ADER scheme possesses the ability to solve MHD supported by problem, and remains high order accuracy both in space and time.

1 Solution Method

1.1 Numerical Scheme in One Dimension

Consider the one dimensional ideal MHD equations of conservation form:

$$\partial_t \boldsymbol{U} + \partial_x \boldsymbol{F}(\boldsymbol{U}) = 0, \tag{1}$$

where

$$\boldsymbol{U} = [\rho, \rho v_x, \rho v_y, \rho v_z, E, B_x, B_y, B_z]^{\mathrm{T}}$$

is the vector of unknown conservative variables and $\boldsymbol{F}(\boldsymbol{U})$ is the flux vector, where ρ is the density, (v_x, v_y, v_z) is the flow speed, (B_x, B_y, B_z) is the magnetic field,

$$E = p/(\gamma-1) + \rho(v_x^2+v_y^2+v_z^2)/2 + (B_x^2+B_y^2+B_z^2)/2$$

is the total energy, and p is the pressure. Integrating Eq. (1) over a space-time control volume in x-t space

$$[x_{i-1/2}, x_{i+1/2}] \times [t^n, t^{n+1}]$$

of dimensions

$$\Delta x = x_{i+1/2} - x_{i-1/2}, \quad \Delta t = t^{n+1} - t^n,$$

we obtain the following one-step finite-volume scheme:

$$\boldsymbol{U}_i^{n+1} = \boldsymbol{U}_i^n + \frac{\Delta t}{\Delta x}(\boldsymbol{F}_{i-1/2} - \boldsymbol{F}_{i+1/2}). \tag{2}$$

Here $\boldsymbol{U}_i^n$ is the cell average of the solution at time level t^n, and can be given by the initial value. $\boldsymbol{F}_{i+1/2}$ is the time average of the physical flux at cell interface $x_{i+1/2}$. They can be given respectively:

$$\boldsymbol{U}_i^n = \frac{1}{\Delta x}\int_{x_{i-1/2}}^{x_{i+1/2}} \boldsymbol{U}(x, t^n)\mathrm{d}x,$$

$$\boldsymbol{F}_{i+1/2} = \frac{1}{\Delta t}\int_{t^n}^{t^{n+1}} \boldsymbol{F}[\boldsymbol{U}(x_{i+1/2}, t)]\mathrm{d}t. \tag{3}$$

For convenience, we replace t by $\tau = t - t^n$. Then we can change the numerical flux as:

$$\boldsymbol{F}_{i+1/2} = \frac{1}{\Delta t}\int_0^{\Delta t} \boldsymbol{F}[\boldsymbol{U}(x_{i+1/2}, \tau)]\mathrm{d}\tau. \tag{4}$$

Then we can obtain the value of $\boldsymbol{U}(x_{i+1/2},\tau)$ as follows:

To evaluate the leading term, we write a Taylor expansion of the interface state in time

$$\boldsymbol{U}(x_{i+1/2},\tau) = \boldsymbol{U}(x_{i+1/2},0^+) + \sum_{k=1}^{K}\Big[\frac{\partial^k}{\partial t^k}\boldsymbol{U}(x_{i+1/2},0^+)\Big]\frac{\tau^k}{k!}, \tag{5}$$

where $\boldsymbol{U}(x_{i+1/2},0^+) = \lim\limits_{t\to 0^+}\boldsymbol{U}(x_{i+1/2},t)$ and K is the order of the approximation.

Eq. (5) consists of two parts: the leading term $\boldsymbol{U}(x_{i+1/2},0^+)$ and the higher order terms $\frac{\partial^k}{\partial t^k}\boldsymbol{U}(x_{i+1/2},0^+)$, which need to be solved respectively. The leading term accounts for the first-instant interaction of the boundary extrapolated values $\boldsymbol{U}_{\rm L}(x_{i+1/2})$ and $\boldsymbol{U}_{\rm R}(x_{i+1/2})$, and can be obtained by the conventional Riemann problem:

$$\partial_t\boldsymbol{U} + \partial_x\boldsymbol{F}(\boldsymbol{U}) = 0;$$
$$\boldsymbol{U}(x,0) = \begin{cases}\boldsymbol{U}_{\rm L}(x_{i+1/2}), & x < x_{i+1/2},\\ \boldsymbol{U}_{\rm R}(x_{i+1/2}), & x > x_{i+1/2}.\end{cases} \tag{6}$$

A key ingredient here is the availability of approximate Riemann solver to provide this first term in the expansion. In this paper, we use the HLL's Riemann solver, which was put forward by Harten, Lax and Van Leer[16].

The higher order terms are evaluated in two steps. First we express all time derivatives via spatial derivatives by means of the Cauchy-Kowalewski procedure[3]. For system Eq. (1) the procedure yields the following expressions:

$$\partial_t\boldsymbol{U} = -\Big(\frac{\partial\boldsymbol{F}}{\partial\boldsymbol{U}}\Big)\partial_x\boldsymbol{U},$$
$$\partial_{tx}\boldsymbol{U} = -\Big(\frac{\partial^2 F}{\partial\boldsymbol{U}^2}\Big)(\partial_x\boldsymbol{U})^2 - \Big(\frac{\partial\boldsymbol{F}}{\partial\boldsymbol{U}}\Big)\partial_{xx}\boldsymbol{U},$$
$$\partial_{tt}\boldsymbol{U} = -\Big(\frac{\partial^2 F}{\partial\boldsymbol{U}^2}\Big)\partial_t\partial_x\boldsymbol{U} - \Big(\frac{\partial\boldsymbol{F}}{\partial\boldsymbol{U}}\Big)\partial_{xt}\boldsymbol{U}, \tag{7}$$

and so on. From Eq. (7), we can obtain all the high order time derivatives required by Eq. (5) if the spatial derivatives are known. Thus, our next step is to calculate the spatial derivatives. The evolution equations for the spatial derivatives can be derived by differentiating the governing Eq. (1). In general, the obtained evolution equation for each spatial derivative

$$\boldsymbol{U}^{(k)} \equiv \frac{\partial^k}{\partial x^k}\boldsymbol{U}, \qquad 1 \leqslant k \leqslant K$$

is in non-conservative form and contains a nonlinear source term H depending on spatial derivatives:

$$\partial_t(\boldsymbol{U}^{(k)}) + \boldsymbol{A}(\boldsymbol{U})\partial_x(\boldsymbol{U}^{(k)}) = H(\boldsymbol{U}^{(0)},\boldsymbol{U}^{(1)},\cdots,\boldsymbol{U}^{(l)}),$$
$$l = 0,\cdots,K-1; \quad k = 1,\cdots,K, \tag{8}$$

where the coefficient matrix $\boldsymbol{A}(\boldsymbol{U})$ is precisely the Jacobian matrix $\frac{\partial\boldsymbol{F}}{\partial\boldsymbol{U}}$. For the Taylor expansion Eq. (5) we need the solution of Eq. (8) for each $k = 1,\cdots,K$ at interface position $x = x_{i+1/2}$ at the time $\tau = 0^+$. Therefore, the source term comes into effect for $\tau > 0$ only, and can be neglected. Additionally, we linearize the equation around the leading term $\boldsymbol{U}(x_{i+1/2},0^+)$ of the time expansion Eq. (5) and replace the piece-wise polynomial initial data by left and right boundary extrapolated values of spatial derivatives at $x_{i+1/2}$. The described simplifications result in the following linear conventional Riemann problem for the spatial derivatives $\boldsymbol{U}^{(k)}$:

$$\partial_t(\boldsymbol{U}^{(k)}) + \boldsymbol{A}_{i+1/2}\partial_x(\boldsymbol{U}^{(k)}) = 0,$$
$$\boldsymbol{A}_{i+1/2} = \boldsymbol{A}[\boldsymbol{U}(x_{i+1/2},0^+)];$$
$$\boldsymbol{U}^{(k)}(x,0) = \begin{cases}\dfrac{\partial^k}{\partial x^k}\boldsymbol{U}_{\rm L}(x_{i+1/2},0^+) \equiv \lim\limits_{t\to 0^+}\dfrac{\partial^k}{\partial x^k}\boldsymbol{U}_{\rm L}(x_{i+1/2},t), & x < x_{i+1/2},\\ \dfrac{\partial^k}{\partial x^k}\boldsymbol{U}_{\rm R}(x_{i+1/2},0^+) \equiv \lim\limits_{t\to 0^+}\dfrac{\partial^k}{\partial x^k}\boldsymbol{U}_{\rm R}(x_{i+1/2},t), & x > x_{i+1/2}.\end{cases} \tag{9}$$

Note that the coefficient matrix $A_{i+1/2}$ is the same for all derivatives and has to be evaluated only once. Then the spatial derivatives $\boldsymbol{U}^{(k)}$ in Eq. (9) are com-

puted as $\boldsymbol{U}^{(k)} = \boldsymbol{U}_*^{(k)}(0)$, with the

$$\boldsymbol{U}^{(k)} = \boldsymbol{U}_*^{(k)}\big[(x - x_{i+1/2})/\tau\big]$$

as the self-similar solution of Eq. (9).

Finally, having found all spatial derivatives we form the Taylor expansion Eq. (5). Then there are two options now existing to evaluate the numerical flux. The first option is the state-expansion ADER[15], in which the approximate state Eq. (5) is inserted into the definition of the numerical flux Eq. (3) and then an appropriate Kth-order accurate quadrature is used for time integration:

$$\boldsymbol{F}_{i+1/2} = \sum_{l=0}^{K_l} \boldsymbol{F}[\boldsymbol{U}(x_{i+1/2}, \gamma_l \Delta t)]\omega_l. \tag{10}$$

Here γ_l and ω_l are properly scaled nodes and weights of the rule and K_α is the number of nodes.

The second option to evaluate the numerical flux is the flux-expansion ADER[5,12], in which we seek Taylor expansion of the physical flux at $x_{i+1/2}$:

$$\begin{aligned}\boldsymbol{F}(x_{i+1/2}, \tau) =& \boldsymbol{F}(x_{i+1/2}, 0^+) + \\ & \sum_{k=1}^{K} \Big[\frac{\partial^k}{\partial t^k}\boldsymbol{F}(x_{i+1/2}, 0^+)\Big]\frac{\tau^k}{k!}.\end{aligned} \tag{11}$$

From Eq. (3) and Eq. (11) the numerical flux is now given by

$$\begin{aligned}\boldsymbol{F}_{i+1/2} =& \boldsymbol{F}(x_{i+1/2}, 0^+) + \\ & \sum_{k=1}^{K} \Big[\frac{\partial^k}{\partial t^k}F(x_{i+1/2}, 0^+)\Big]\frac{\Delta t^k}{(k+1)!}.\end{aligned} \tag{12}$$

The leading term $F(x_{i+1/2}, 0^+)$ accounts for the first interaction of left and right boundary extrapolated values and is computed as a certain monotone flux of the conventional Riemann problem Eq. (6) for the leading term of the state expansion Eq. (5). The remaining higher order time derivatives of the flux in Eq. (12) are expressed via time derivatives of the intercell state $\dfrac{\partial^k}{\partial t^k}\boldsymbol{U}(x_{i+1/2}, 0^+)$, which are known from Eq. (5).

In our calculations, we choose the second option Eq. (12). And then, the solution is advanced in time by updating the cell averages according to the one-step formula Eq. (2).

1.2 Numerical Scheme in Two Dimensions

The process is the same as one-dimensional situation. Consider the following two dimensional nonlinear system of conservation laws:

$$\partial_t \boldsymbol{U} + \partial_x \boldsymbol{F}(\boldsymbol{U}) + \partial_y \boldsymbol{G}(\boldsymbol{U}) = 0. \tag{13}$$

Integration of Eq. (13) over a space-time control volume of dimensions

$$\begin{aligned}\Delta x &= x_{i+1/2} - x_{i-1/2}, \\ \Delta y &= y_{j+1/2} - y_{j-1/2}, \\ \Delta t &= t^{n+1} - t^n\end{aligned}$$

produces the following one-step finite-volume scheme:

$$\begin{aligned}\boldsymbol{U}_{i,j}^{n+1} =& \boldsymbol{U}_{i,j}^n + \frac{\Delta t}{\Delta x}(\boldsymbol{F}_{i-1/2,j} - \boldsymbol{F}_{i+1/2,j}) + \\ & \frac{\Delta t}{\Delta y}(\boldsymbol{G}_{i,j-1/2} - \boldsymbol{G}_{i,j+1/2}).\end{aligned} \tag{14}$$

Here $\boldsymbol{U}_{i,j}^n$ is the cell average of the solution at time level:

$$\boldsymbol{U}_{i,j}^n = \frac{1}{\Delta x}\frac{1}{\Delta y}\int_{x_{i-1/2}}^{x_{i+1/2}} \int_{y_{j-1/2}}^{y_{j+1/2}} \boldsymbol{U}(x, y, t^n)\mathrm{d}y\mathrm{d}x. \tag{15}$$

And $\boldsymbol{F}_{i+1/2,j}$, $\boldsymbol{G}_{i,j+1/2}$ are the space-time averages of the physical fluxes at the cell interfaces:

$$\begin{aligned}\boldsymbol{F}_{i+1/2,j} =& \frac{1}{\Delta t}\frac{1}{\Delta y} \cdot \\ & \int_{y_{j-1/2}}^{y_{j+1/2}} \int_{t^n}^{t^{n+1}} \boldsymbol{F}[\boldsymbol{U}(x_{i+1/2}, y, t)]\mathrm{d}t\mathrm{d}y, \\ \boldsymbol{G}_{i,j+1/2} =& \frac{1}{\Delta t}\frac{1}{\Delta x} \cdot \\ & \int_{x_{i-1/2}}^{x_{i+1/2}} \int_{t^n}^{t^{n+1}} \boldsymbol{G}(\boldsymbol{U}(x, y_{j+1/2}, t))\mathrm{d}t\mathrm{d}x.\end{aligned} \tag{16}$$

While describing the procedure to evaluate the numerical flux in two dimensions we concentrate on $\boldsymbol{F}_{i+1/2,j}$; the expression for $\boldsymbol{G}_{i,j+1/2}$ is obtained in an entirely analogous manner.

The evaluation of the ADER numerical flux consists of the following steps. First we discretize the spatial integrals over the cell faces in Eq. (16) using a tensor product of a suitable Gaussian numerical quadrature. The expression for the numerical flux

in the x coordinate direction then reads

$$\boldsymbol{F}_{i+1/2,j}=\sum_{\alpha=1}^{N}\left\{\frac{1}{\Delta t}\int_{t^n}^{t^{n+1}}\boldsymbol{F}\big[\boldsymbol{U}(x_{i+1/2},y_\alpha,t)\big]\mathrm{d}t\right\}K_\alpha. \tag{17}$$

Where y_α is the integration points over the cell face $[y_{j-1/2},y_{j+1/2}]$ and K_α is the weights computed by the Gauss numerical quadrature. Normally, we use the two-point Gaussian quadrature for third and fourth order schemes and a higher-order Gaussian quadrature for fifth and higher order schemes.

The following steps are provided only for x-direction computation and the same procedure follows for y-direction computation.

We write Taylor series expansion in time

$$\begin{aligned}&\boldsymbol{U}(x_{i+1/2},y_\alpha,\tau)=\\&\quad\boldsymbol{U}(x_{i+1/2},y_\alpha,0^+)+\\&\quad\sum_{k=1}^{K}\Big[\frac{\partial^k}{\partial t^k}\boldsymbol{U}(x_{i+1/2},y_\alpha,0^+)\Big]\frac{\tau^k}{k!},\end{aligned} \tag{18}$$

where $\tau=t-t^n$. The leading term $\boldsymbol{U}(x_{i+1/2},y_\alpha,0^+)$ is the Godunov state of the conventional Riemann problem

$$\begin{aligned}&\partial_t\boldsymbol{U}+\partial_x\boldsymbol{F}(\boldsymbol{U})=0;\\&\boldsymbol{U}(x,y_\alpha,0)=\begin{cases}\boldsymbol{U}_{\mathrm{L}}(x_{i+1/2},y_\alpha), & x<x_{i+1/2},\\ \boldsymbol{U}_{\mathrm{R}}(x_{i+1/2},y_\alpha), & x>x_{i+1/2}.\end{cases}\end{aligned} \tag{19}$$

To evaluate higher-order terms we first express all time derivatives by spatial derivatives by means of the Cauchy-Kowalewski procedure. We can derive homogeneous evolution equations and the initial conditions for each spatial derivative

$$\boldsymbol{U}^{(k+l)}\equiv\frac{\partial^{k+l}}{\partial x^k\partial y^l}\boldsymbol{U},\quad 1\leqslant k+l\leqslant K. \tag{20}$$

The spatial derivatives at $(x-x_{i+1/2})/\tau=0$ are then the Godunov states of the following linearized Riemann problem with piece-wise constant initial data:

$$\begin{aligned}&\partial_t(\boldsymbol{U}^{(k+l)})+\boldsymbol{A}_{i+1/2}\partial_x(\boldsymbol{U}^{(k+l)})=0,\\&\boldsymbol{A}_{i+1/2}=\boldsymbol{A}[\boldsymbol{U}^{(k+l)}(x_{i+1/2},0^+)];\\&\boldsymbol{U}^{(k+l)}(x,y_\alpha,0)=\end{aligned}$$

$$\begin{cases}\dfrac{\partial^{k+l}}{\partial x^k\partial y^l}\boldsymbol{U}_{\mathrm{L}}(x_{i+1/2},y_\alpha,0^+)\equiv\\ \quad\lim\limits_{t\to0^+}\dfrac{\partial^{k+l}}{\partial x^k\partial y^l}\boldsymbol{U}_{\mathrm{L}}(x_{i+1/2},y_\alpha,t),\\ \qquad x<x_{i+1/2},\\ \dfrac{\partial^{k+l}}{\partial x^k\partial y^l}\boldsymbol{U}_{\mathrm{R}}(x_{i+1/2},y_\alpha,0^+)\equiv\\ \quad\lim\limits_{t\to0^+}\dfrac{\partial^{k+l}}{\partial x^k\partial y^l}\boldsymbol{U}_{\mathrm{R}}(x_{i+1/2},y_\alpha,t),\\ \qquad x>x_{i+1/2}.\end{cases} \tag{21}$$

After solving Eq. (20) for $1\leqslant k+l\leqslant K$, we form the Taylor expansion Eq. (18) for the interface state at the Gaussian integration point $(x_{i+1/2},y_\alpha)$. The flux of the state-expansion ADER scheme is obtained by inserting the approximate state Eq. (18) into formula Eq. (17) and using an appropriate Kth-order accurate quadrature for time integration:

$$\boldsymbol{F}_{i+1/2,j}=\sum_{\alpha=1}^{N}\sum_{l=1}^{N}[\boldsymbol{F}(\boldsymbol{U}(x_{i+1/2},y_\alpha,\tau))K_l]K_\alpha. \tag{22}$$

For the flux expansion ADER schemes we write Taylor time expansion of the physical flux at each point

$$\begin{aligned}&\boldsymbol{F}(x_{i+1/2},y_\alpha,\tau)=\\&\qquad\boldsymbol{F}(x_{i+1/2},y_\alpha,0^+)+\\&\qquad\sum_{k=1}^{K}\Big[\frac{\partial^k}{\partial t^k}\boldsymbol{F}(x_{i+1/2},y_\alpha,0^+)\Big]\frac{\tau^k}{k!}.\end{aligned} \tag{23}$$

From Eq. (16) and Eq. (22) the numerical flux is given by

$$\begin{aligned}&\boldsymbol{F}_{i+1/2}=\\&\boldsymbol{F}(x_{i+1/2},y_\alpha,0^+)+\\&\sum_{k=1}^{K}\Big[\frac{\partial^k}{\partial t^k}\boldsymbol{F}(x_{i+1/2},y_\alpha,0^+)\Big]\frac{\Delta t^k}{(k+1)!}.\end{aligned} \tag{24}$$

Entirely analogous to the one-dimensional case, the leading term $\boldsymbol{F}(x_{i+1/2},y_\alpha,0^+)$ is computed from Eq. (19) using a monotone upwind flux. The remaining higher order time derivatives of the flux in Eq. (22) are expressed via time derivatives of the intercell state $\boldsymbol{U}(x_{i+1/2},y_\alpha,0^+)$ which are given by the Taylor expansion Eq. (18). The solution is advanced in time by updating the cell averages according to the one-step formula Eq. (14).

In the ADER scheme solving method, the key process is to solve the Riemann problem. There are many methods to solve the Riemann problem, such as the MUSCL (Monotone Upstream-centered Schemes for Conservation Laws) scheme[17], PPM (piecewise parabolic method) scheme[18], and HLL scheme[13]. The HLL scheme used in the present paper to solve the Riemann problem can be described as follows:

$$\partial_t \boldsymbol{U} + \partial_x \boldsymbol{F}(\boldsymbol{U}) = 0;$$

$$\boldsymbol{U}(x,0) = \begin{cases} \boldsymbol{U}_{\rm L}(x_{i+1/2}), & x < x_{i+1/2}, \\ \boldsymbol{U}_{\rm R}(x_{i+1/2}), & x > x_{i+1/2}. \end{cases} \tag{25}$$

The interface value and the numeral flux have the form as:

$$\boldsymbol{U}(x_{i+1/2},0^+) = \begin{cases} \boldsymbol{U}_{\rm L}, & b_i^{\rm L} \geqslant x/t; \\ \boldsymbol{U}^*, & b_i^{\rm L} \leqslant x/t \leqslant b_i^{\rm R}; \\ \boldsymbol{U}_{\rm R}, & b_i^{\rm R} \leqslant x/t. \end{cases} \tag{26}$$

$$\boldsymbol{F}(x_{i+1/2},0^+) = \begin{cases} \boldsymbol{F}(\boldsymbol{U}_{\rm L}), & b_i^- \geqslant 0; \\ \boldsymbol{F}^*, & b_i^- \leqslant 0 \leqslant b_i^+; \\ \boldsymbol{F}(\boldsymbol{U}_{\rm R}), & b_i^+ \leqslant 0. \end{cases} \tag{27}$$

where

$$\boldsymbol{U}^*(x_{i+1/2},0^+) = \frac{1}{b_i^{\rm R} - b_i^{\rm L}}\big\{b_i^{\rm R}\boldsymbol{U}_{\rm R} - b_i^{\rm L}\boldsymbol{U}_{\rm L} - [\boldsymbol{F}(\boldsymbol{U}_{\rm R}) - \boldsymbol{F}(\boldsymbol{U}_{\rm L})]\big\}, \tag{28}$$

$$\boldsymbol{F}^*(x_{i+1/2},0^+) = \frac{1}{b_i^+ - b_i^-}\big\{b_i^+\boldsymbol{F}(\boldsymbol{U}_{\rm L}) - b_i^-\big[\boldsymbol{F}(\boldsymbol{U}_{\rm R})\big]\big\} + \frac{b_i^+ b_i^-}{b_i^+ - b_i^-}(\boldsymbol{U}_{\rm R} - \boldsymbol{U}_{\rm L}), \tag{29}$$

$$\begin{aligned} b_i^{\rm R} &= \max\{\bar{v}_{xi} + \bar{c}_{{\rm f}xi}, v_{x{\rm R}} + c_{{\rm f}xi{\rm R}}\}, \\ b_i^{\rm L} &= \max\{\bar{v}_{xi} - \bar{c}_{{\rm f}xi}, v_{x{\rm L}} - c_{{\rm f}xi{\rm L}}\}, \\ b_i^+ &= \max\{b_i^{\rm R}, 0\}, \\ b_i^- &= \min\{b_i^{\rm L}, 0\}, \end{aligned} \tag{30}$$

where $\bar{v}_{xi}$ and $\bar{c}_{{\rm f}xi}$ are the Roe average of velocity and fast magnetic sound velocity.

$$\bar{\rho}_i = \frac{\sqrt{\rho_{\rm L}}\rho_{\rm L} + \sqrt{\rho_{\rm R}}\rho_{\rm R}}{\sqrt{\rho_{\rm L}} + \sqrt{\rho_{\rm R}}},$$

$$\bar{v}_{\alpha i} = \frac{\sqrt{\rho_{\rm L}}v_{\alpha{\rm L}} + \sqrt{\rho_{\rm R}}v_{\alpha{\rm R}}}{\sqrt{\rho_{\rm L}} + \sqrt{\rho_{\rm R}}}, \quad \alpha = x, y, z$$

$$\bar{B}_{\beta i} = \frac{\sqrt{\rho_{\rm L}}B_{\beta{\rm R}} + \sqrt{\rho_{\rm R}}B_{\beta{\rm L}}}{\sqrt{\rho_{\rm L}} + \sqrt{\rho_{\rm R}}}, \quad \beta = x, y, z$$

$$\bar{H}_i = \frac{\sqrt{\rho_{\rm L}}H_{\rm L} + \sqrt{\rho_{\rm R}}H_{\rm R}}{\sqrt{\rho_{\rm L}} + \sqrt{\rho_{\rm R}}}.$$

Here H is the enthalpy, has the form as:

$$\rho H = E + p + B^2/2 = \frac{\gamma p}{\gamma - 1} + \rho v^2/2 + B^2,$$

where $v^2 = v_x^2 + v_y^2 + v_z^2$ and $B^2 = B_x^2 + B_y^2 + B_z^2$, then the Roe average are:

$$\bar{v}^2 = \bar{v}_x^2 + \bar{v}_y^2 + \bar{v}_z^2,$$
$$\bar{B}^2 = \bar{B}_x^2 + \bar{B}_y^2 + \bar{B}_z^2.$$

The fast magnetic sound velocity

$$c_{{\rm f}xi} \equiv c_{{\rm f}xi}(\rho_i, v_{\alpha i}, B_{\beta i}, H_i) = \sqrt{(a_*^2 + \sqrt{a_*^4 - 4(\gamma p B_x^2)/\rho^2})/2}\,,$$

where

$$a_*^2 = (\gamma p + B^2)/\rho,$$

and then

$$\bar{c}_{{\rm f}xi} = c_{{\rm f}xi}(\bar{\rho}_i, \bar{v}_{\alpha i}, \bar{B}_{\beta i}, \bar{H}_i).$$

2 Numerical Results

2.1 Brio-Wu Shock Tube Problem

Proposed by Brio and Wu[19−20], this MHD problem has been a benchmark test for solving the one dimensional ideal MHD equations. Similar to Sod's shock-tube problem[19], the initial condition is composed of two distinct constant states:

$$\rho_1 = 1.0, \quad u_1 = 0.0, \quad v_1 = 0.0,$$
$$p_1 = 1.0, \quad B_{y1} = 1.0;$$
$$\rho_2 = 0.125, \quad u_2 = 0.0, \quad v_2 = 0.0,$$
$$p_2 = 0.1, \quad B_{y2} = -1.0.$$

In addition, $B_x = 0.75$, $\gamma = 2.0$ is a constant value in the whole domain [0, 1]. According to Brio and Wu *et al.*[19], numerical solutions with a uniform mesh of 800 grid points and the CFL=0.8 are obtained. Figure 1(a)∼(d) show numerical solution of density, velocity v_x, magnetic field B_y and pressure at 400 time steps. From this figure, we can see that the

wave family consists of right-moving and left-moving waves. The left-moving waves are a fast rarefaction wave, denoted by FR in the figure, and a slow compound wave, denoted by SM. The right-moving waves included a contact discontinuity, denoted by C, a Slow Shock (SS), and a Fast Rarefaction wave, FR. Our result shows sharp resolution of all shock waves.

Figure 1(e) shows the result of grid refinement study, in which 400, 800, 1600 grid points are used. And the CFL number used for these three calculations is the same. It is clear to see that, mesh refinement can improve numerical accuracy.

2.2 Dai-Woodward Shock Tube Problem

Dai and Woodward's shock tube problem has been studied by Dai and Woodward[21] and Bouchut *et al.*[20] The initial data[20] are given as:

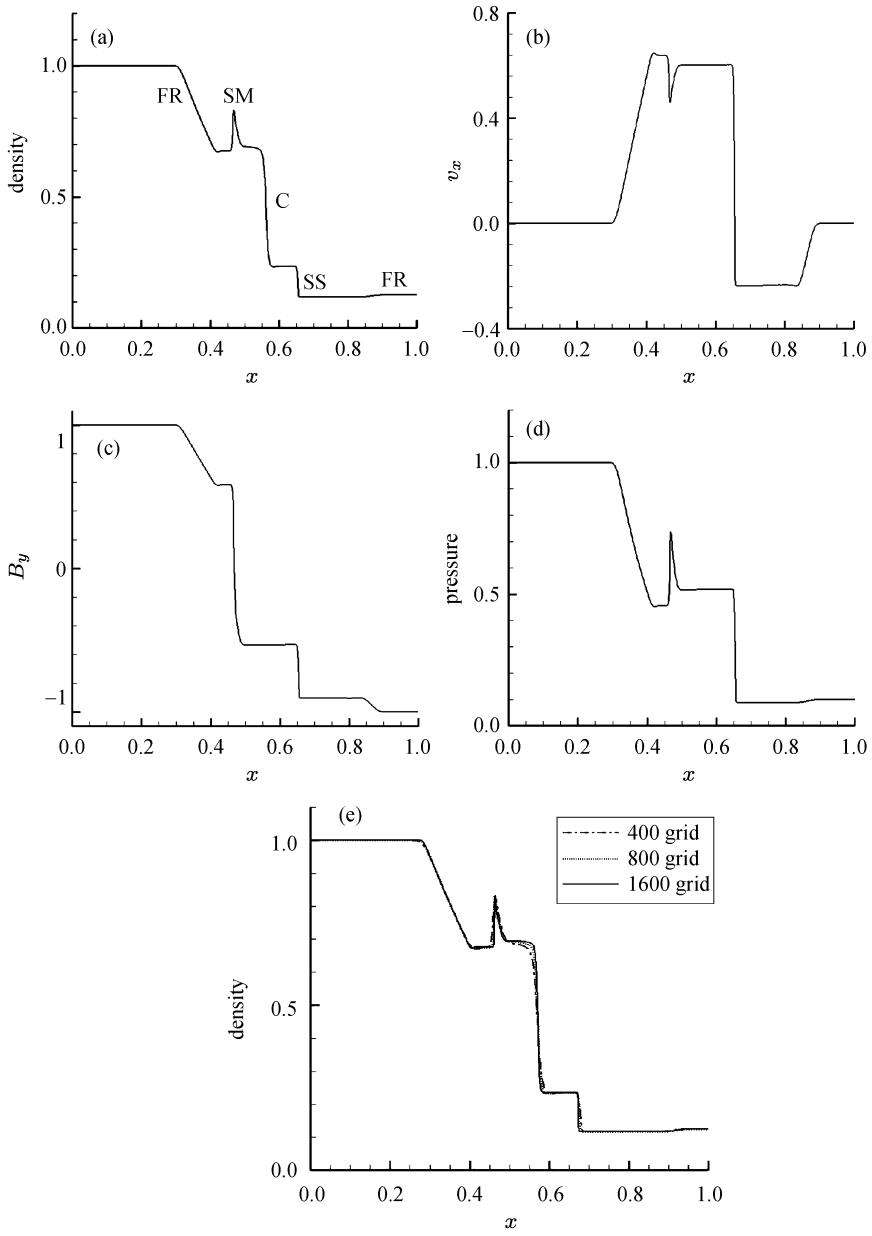

Fig. 1 MHD solution by ADER scheme for Brio-Wu shock tube problem. (a) density profile, (b) velocity v_x profile, (c) magnetic field B_y profile, (d) pressure profile, (e) comparison between different resolutions

$$\rho_{\rm l} = 1.08, \quad v_{x\rm l} = 1.2, \quad v_{y\rm l} = 0.01, \quad v_{z\rm l} = 0.5,$$
$$p_{\rm l} = 0.95, \quad B_{y\rm l} = 3.6/\sqrt{4\pi}, \quad B_{z\rm l} = 2/\sqrt{4\pi};$$
$$\rho_{\rm r} = 1.0, \quad v_{x\rm r} = 0.0, \quad v_{y\rm r} = 0.0, \quad v_{z\rm r} = 0.0,$$
$$p_{\rm r} = 1.0, \quad B_{y\rm r} = 4/\sqrt{4\pi}, \quad B_{z\rm r} = 2/\sqrt{4\pi}.$$

In addition, $B_x = 4/\sqrt{4\pi}$, $\gamma = 2$ is a constant value in the whole domain [0, 1] with a uniform mesh of 1000 grid points, and the CFL number is set to be 0.45. Figure 2(a)∼(d) show numerical solution of density, velocity v_y, magnetic field B_y and pressure at $t = 0.15$. There are seven discontinuities in this case: the left moving, a fast shock, a slow shock and a rotational discontinuity; the right moving, a fast shock, a slow shock, a rotational discontinuity and a contact discontinuity.

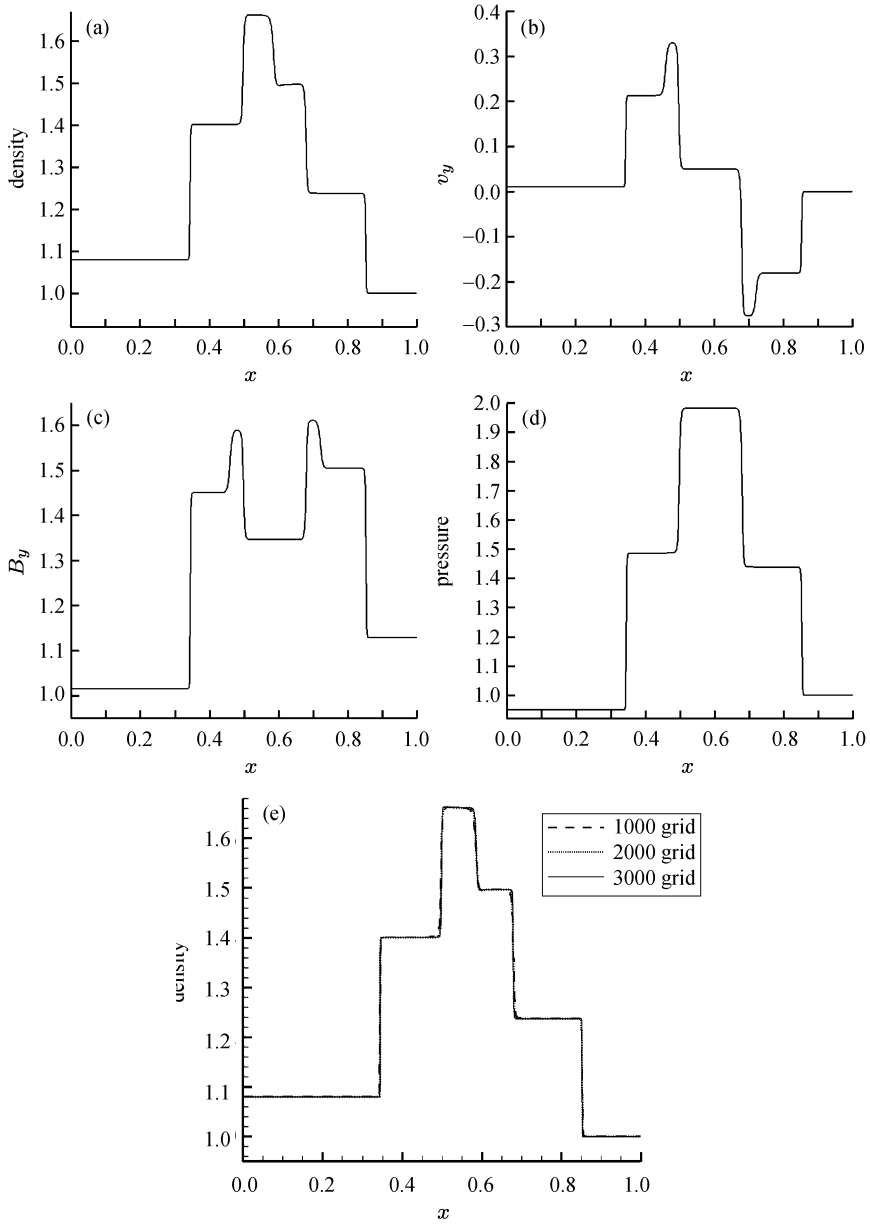

Fig. 2 MHD solution by ADER scheme for Dai-Woodward shock tube problem. (a) density profile, (b) velocity v_y profile, (c) magnetic field B_y profile, (d) pressure profile, (e) comparison between different resolution

By comparison with that of Bouchut *et al.*'s results[20], again the MHD solution with ADER scheme is quite good. Under the same CFL condition, different resolutions have been examined with 1000, 2000, 3000 grid points respectively. Figure 2(e) shows comparison of density profiles. The accuracy is nearly the same with different resolution. So in this case, the mesh refinement does not improve numerical accuracy.

2.3 Orszag-Tang MHD Vortex Problem

As our preliminary effort to apply the ADER method for multidimensional MHD problem, the Orszag-Tang MHD vortex problem[22] is adopted here. This compressible flow proposed by Orszag and Tang contains significant features of MHD turbulence, and has been taken as a standard numerical test[22−26]. The flow involves complex evolution due to interactions between shock waves and the vortices. The initial conditions are as follows:

$$(\rho, v_x, v_y, p, B_x, B_y) = \{\gamma^2, -\gamma\sin(\pi y), \gamma\sin(\pi x), \gamma, -\sin(\pi y), \sin(2\pi x)\}.$$

Here we used $\gamma = 5/3$. The problem was calculated with a CFL number of 0.2. The computational domain is $[0, 2\pi] \times [0, 2\pi]$ with periodic boundary condition in both x and y directions. According to Zhang *et al.*[25], we use a uniform mesh of 200×200 grid points. We have successfully run our calculation from $t = 0.5$ to $t = 3$, which is the final time in most of previously published results. Figure 3(a), 3(b) show the density and pressure contours at $t = 0.5$ using the same contour level as those in Jiang and Wu[26]. Clearly, our results are similar to Jiang and Wu's results.

For the sake of comparison, we show the density contours at $t = 0.5$, $t = 1$, and $t = 3$ using the same contour level, shown in Figure 3(a) (c) (d) respectively. Figure 3(a) (c) (d) show very complex shock structure. At $t = 1$, an intermediate shock is formed at the shock front in the region of $\pi < x < 1.5\pi$ and $0 < y < 0.75\pi$.

To compare the mesh refinement, we calculated the density of 200×200, 300×300 and 400×400 grid points, see Figure 3(c) (e) (f). Evidently, these results are similar to those obtained formerly[22−26]. It is clear that the effect of mesh refinement is not very palpable. In MHD simulation, how to control the numerical error of magnetic field divergence is a challenge[27]. In order to see how this numerical error evolves, Figure 3(g) expresses the evolution of the $\nabla \cdot \boldsymbol{B}$ numerical error along with time in different mesh point, in which error $E = \frac{\sum_{k=1}^{M} |(\nabla \cdot \boldsymbol{B})_k|}{M}$ (M is the number of mesh nodes in the computational domain)[27]. This figure tells that the numerical error of magnetic field divergence is tolerable.

2.4 Comparison Between HLL and ADER

In order to see the difference of ADER scheme and HLL scheme, we calculate the following cases: using second-order HLL method only and ADER method introduced in Section 2, respectively. We test Brio-Wu shock tube problem through these two methods. Figure 4(a) (b) are the density solved by HLL scheme and ADER scheme with CFL= 0.3 and CFL= 0.6 at $t = 0.1$. Through the two figures we can see that, when the Courant-Friedrichs-Lewy (CFL) number is small, the two methods show no differences. But when the CFL number is large, the HLL scheme turns up some oscillation at the slow shock, while the ADER scheme does a good job. In conclusion, the HLL scheme has higher oscillatory result, when CFL number is large, and the ADER scheme can avoid this oscillatory and capture the shock for large CFL number.

3 Conclusion

In this paper, we have presented the ADER scheme for ideal MHD equations in one and two spatial dimension. Contrast to modern Godunov-type, the ADER method is one-step, fully discrete scheme for which the reconstruction procedure is carried out only once per time step, and can be implemented in the

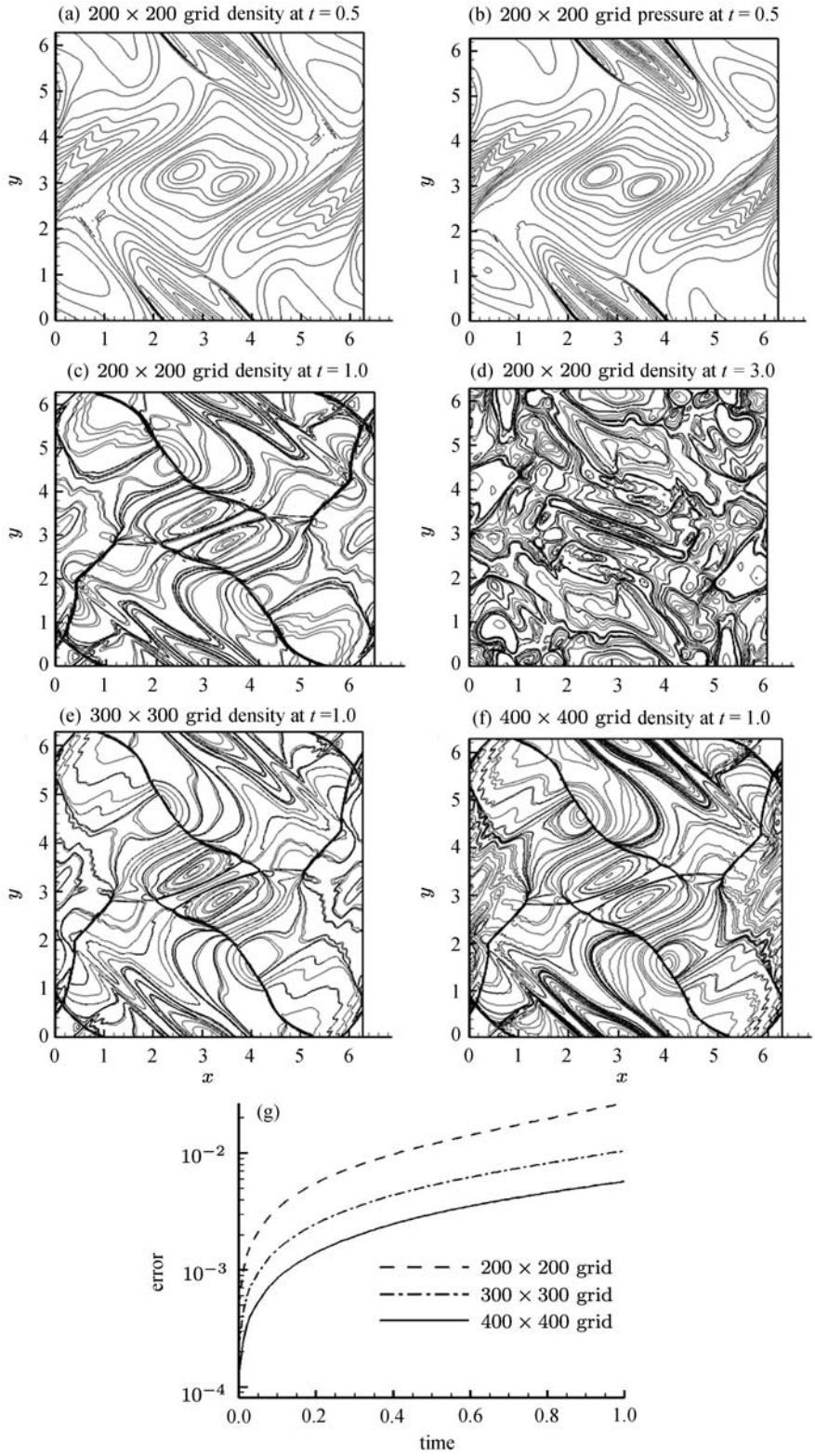

Fig. 3 MHD solution by the ADER method for Orszag-Tang MHD vortex problem. (a) Density contours of 200 ×200 grid points at $t = 0.5$. (b) Pressure contours of 200×200 grid points at $t = 0.5$. (c) Density contours of 200×200 grid points at $t = 1.0$. (d) Density contours of 200×200 grid points at $t = 3.0$. (e) Density contours of 300×300 grid points at $t = 1.0$. (f) Density contours of 400×400 grid points at $t = 1.0$. (g) Evolution of the error for $\nabla \cdot \boldsymbol{B}$ in the three cases of the mesh refinement

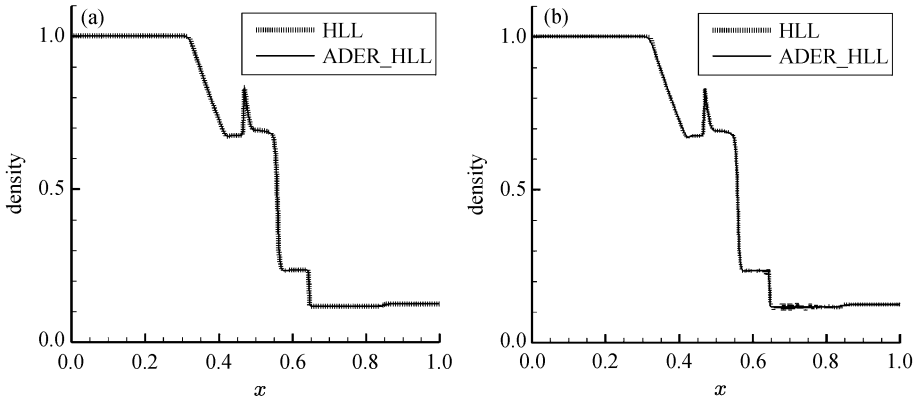

Fig. 4 Density for one dimension Brio-Wu shock tube problem at time $t = 0.1$ for 1000 grid points. (a) CFL=0.3, (b) CFL=0.6

framework of finite volumes and discontinuous Galerkin finite elements. Several standard MHD problems have been solved, including Brio-Wu shock tube problem, Dai-Woodward shock tube problem, and Orszag-Tang MHD vortex problem. In all cases, the numerical results by ADER method appears precise non-oscillation results, and remains high order accuracy both in space and time in the capture of the shock. Through the last compared case, the second-order HLL scheme's result may produce oscillation at the slow shock when the CFL number is very large, such as CFL = 0.6, seeing Figure 4(b). However the ADER scheme can restrain the oscillation and obtain the high order non-oscillatory result. Meanwhile, the numerical error of magnetic field divergence can be kept to a tolerable range without any special treatment of magnetic field divergence cleaning procedure. In conclusion, the ADER scheme can be applied in the MHD numerical simulation, and keeps very high order accuracy both in space and time.

According to these conclusions, future applications of the ADER scheme to the MHD numerical simulations will be a promising work, such as its applications to magnetic reconnection, solar wind simulation and solar disturbances in solar-terrestrial space[23,27−28]. At the same time, improving the ADER scheme's order by using different reconstruction methods, such as Essentially Non-Oscillatory (ENO), WENO or CWENO scheme[23,29−34], is also an emphasis in future work.

Reference

[1] Godunov S K. A finite difference method for the computation of discontinuous solutions of the equations of fluid dynamics [J]. *Mat. Sbornik*, 1959, **47**:357-393

[2] Godunov S K. Feodoritova O B, Zhukov V T. A method for computing invariant subspaces of symmetric hyperbolic systems [J]. *J. Comp. Maths Math. Phys.*, 2006, **46**(6):971-982

[3] Toro E F. Riemann solvers and numerical methods for fluid dynamics [M]. New York: Springer Verlag, 1999

[4] Ben-Artzi M, Falcovitz J. A second-order Godunov-type scheme for compressible fluid dynamics [J]. *J. Comp. Phys.*, 1984, **55**:1-32

[5] Toro E F, Titarev V A. Solution of the generalised Riemann problem for advection-reaction equations [J]. *Proc. Roy. Soc. Lond: A*, 2002, **458**(2018):271-281

[6] Titarev V A, Toro E F. ADER scheme for three-dimensional nonlinear hyperbolic systems [J]. *J. Comp. Phys.*, 2005, **204**:715-736

[7] Toro E F, Millington R C, Nejad L A M. Towards very high order Godunov schemes//Godunov Methods: Theory and Applications [M]. Holland: Kluwer Academic/Plenum Publishers, 2001. 905-937

[8] Titarev V A, Toro E F. High order ADER schemes for the scalar advection-reaction-diffusion equations [J]. *CFD J.*, 2003, **12**(1):1-6

[9] Toro E F, Titarev V A. TVD Fluxes for the high-order ADER schemes [J]. *J. Sci. Comp.*, 2003, **24**: 285-309

[10] Schwartzkopff T, Munz C D, Toro E F, Millington R C. ADER-2D: a high-order approach for linear hyperbolic systems in 2D [J]. *J. Sci. Comp.*, 2002, **17**:231-240

[11] Schwartzkopff T, Dumbser M, Munz C D. Fast high order ADER schemes for linear hyperbolic equations [J]. *J. Comp. Phys.*, 2004, **197**:532-539

[12] Takakura Y, Toro E F. Arbitrarily accurate non-oscillatory schemes for a nonlinear conservation law [J]. *CFD J.*, 2002, **11**(1):7-18

[13] Titarev V A, Toro E F. ADER schemes for scalar nonlinear hyperbolic conservation laws with source terms in three space dimensions [J]. *J. Comp. Phys.*, 2005, **202**:196-215

[14] Eleuterio F Toro, Arturo Hidalgo. ADER finite volume schemes for nonlinear reaction-diffusion equations [J]. *Appl. Num. Math.*, 2009, **59**:73-100

[15] Titarev V A, Toro E F. ADER: Arbitrary high order Godunov approach [J]. *J. Sci. Comp.*, 2002, **17**:609-618

[16] Harten A, Lax P D, Van Leer B. On upstream differencing and Godunov-type schemes for hyperbolic conservation laws [J]. *SIAM Rev.*, 1983, **25**(1):35-61

[17] Christophe Berthon. Robustness of MUSCL schemes for 2D unstructured meshes [J]. *J. Comp. Phys.*, 2006, **218**(2):495-509

[18] Colella P, Sekora Michael D. A limiter for PPM that preserves accuracy at smooth extrema [J]. *J. Comp. Phys.*, 2008, **227**:7069-7076

[19] Brio M, Wu C C. An upwind differencing scheme for the equations of ideal magnetohydrodynamics [J]. *J. Comp. Phys.*, 1988, **75**:400-422

[20] Francois Bouchut, Christian Klingenberg, Knut Waagan. A multiwave approximate Riemann solver for ideal MHD based on relaxation II: numerical implementation with 3 and 5 waves [J]. *J. Num. Math.*, 2010, **115**(4):647-679

[21] Dai Wenlong, Woodward Paul R. An approximate Riemann solver for ideal magnetohydrodynamics [J]. *J. Comp. Phys.*, 1994, **111**(2):354-372

[22] Orszag S A, Tang C M. Small-scale structure of two-dimensional magnetohydrodynamic turbulence [J]. *J. Fluid. Mech.*, 1979, **90**:129-143

[23] Feng Xueshang, Zhou Yufen, Hu Yanqi, A 3rd order WENO GLM-MHD scheme for magnetic reconnection [J]. *Chin. J. Space Sci.*, 2006, **26**(1):1-7

[24] Jiang Chaowei, Feng Xueshang, Zhang Jian, Zhong Dingkun. AMR simulations of magnetohydrodynamic problems by the CESE method in curvilinear coordinates [J]. *Solar Phys.*, 2010, **267**:463-491

[25] Zhang Moujin S C, Henry Lin S T, Yu John. Application of the Space-Time Conservation Element and Solution Element Method to the Ideal Magnetohydrodynamic Equations [R]. AIAA 2002-3888

[26] Jiang G S, Wu C C. A high-order WENO finite difference scheme for the equations of ideal magneto-hydrodynamics [J]. *J. Comp. Phys.*, 1999, **150**:561-594

[27] Feng Xueshang, Zhou Yufen, Wu S T. A novel numerical implementation for solar wind modeling by the modified conservation element/solution element method [J]. *Astron. Phys. J.*, 2007, **655**:1110-1126

[28] Feng Xueshang, Yang Liping, Xiang Changqing, Wu S T, Yufen Zhou, Zhong DingKun. Three-dimensional solar wind modeling from the Sun to Earth by a SIP-CESE MHD model with a six-component grid [J]. *Astron. Phys. J.*, 2010, **723**(1):300-319

[29] Harten A, Engquist B, Osher S, Chakravrthy S. Uniformly high-order accurate essentially nonoscillatory schemes, III [D]. *J. Comp. Phys.*, 1987, **71**:231-303

[30] Gottlieb S, Mullen J S. An Implicit WENO Scheme for Steady-State Computation of Scalar Hyperbolic Equations, in Computational Fluid and Solid Mechanics 2003 (ed. K.J. Bathe).

[31] Zhang Yongtao, Shu Chiwang. Third order WENO scheme on three dimensional tetrahedral meshes [J]. *Commun. Comp. Phys.*, 2009, **5**:836-848

[32] Kleimann J, Kopp A, Fichtner H, Grauer R. A novel code for numerical 3-D MHD studies of CME expansion [J]. *Ann. Geophys.*, 2009, **27**:989-1004

[33] Kleimann J, Kopp A, Horst Fichtner, Rainer Grauer. Three-dimensional MHD high-resolution computations with CWENO employing adaptive mesh refinement [J]. *Comp. Phys. Commun.*, 2004, **158**:47-56

[34] Cai Li, Feng Jianhu, Xie Wenxian. A CWENO-type central-upwind scheme for ideal MHD equations [J]. *Appl. Math. Comp.*, 2005, **168**:600-612